# Algorithm of Linear Induction Motor Control for Low Normal Force of Magnetic Levitation Train Propulsion System

Hyunuk Seo[1], Jaewon Lim[2], Gyu-Ha Choe[1], Jang-Young Choi[3], and Jae-Hoon Jeong[3]

[1]Department of Electrical Engineering, Konkuk University, Seoul 05029, South Korea
[2]Department of Magnetic Levitation and Linear Drive, Korea Institute of Machinery and Materials, Daejeon 34103, South Korea
[3]Department of Electrical Engineering, Chungnam National University, Daejeon 34134, South Korea

**This paper presents the analyses and experimental results of a single-sided linear induction motor (SLIM) thrust and normal force for the propulsion of semi-high-speed magnetic levitation (maglev) trains. These trains are composed of a levitation system that uses electromagnetic suspension and a propulsion system that uses SLIMs. The propulsion system of maglev trains using SLIMs has better low noise and dynamic characteristics compared with those using rotators. However, it has nonlinear characteristics due to the effect of slip that occur in the secondary eddy-current induction process; the normal force generated by the SLIM can negatively affect the levitation control. Therefore, a new slip-control algorithm is proposed for the safe operation of maglev trains, reflecting the normal force of the motor in propulsion control. First, the SLIM thrust and normal force are analyzed through the finite-element method (FEM) for a precise analysis of the slips. Furthermore, a slip range with a low normal force was derived based on the FEM analysis results, and these results are reflected in the propulsion control algorithm. Finally, the new algorithm was validated by an application to a full-sized testing apparatus.**

*Index Terms*—**Levitation, magnetic levitation (maglev), normal force, power consumption, propulsion.**

## I. Introduction

SINGLE-SIDED linear induction motors (SLIMs) have advantages such as the construction costs, high initial thrusts, simple structures, flexible mechanisms, absence of dust emission, and low noise [1]. Thus, they are widely adopted as traction components in several industrial applications, particularly in magnetic levitation (maglev) transportation systems or urban subway systems. They can provide higher passenger comfort with lower noise, because SLIM is that it generates linear motions without rotary-to-linear motion conversion devices [2].

The 200 km/h-class semi-high-speed maglev train, which is under development in Korea, uses SLIMs for the propulsion system because they are lightweight and inexpensive. However, their driving characteristics are inferior to those of linear synchronous motors due to their low power factor and efficiency. In addition, they generate a normal force perpendicular to the moving direction, according to the slip frequency and thrust, which has adverse effects on the levitation system. The normal force in the SLIM can be described by the relationship between the thrust and slip [3].

The normal force can be reduced by adjusting the slip frequency [4]. However, one disadvantage of the constant slip frequency operation is that the best performance cannot be achieved because the optimized slip frequency is determined based on the force and the normal force at each speed. Because the slip is determined according to the speed in consideration of the normal force, it cannot be operated at the optimum driving condition in terms of propulsion efficiency. Therefore, to increase the stability of the levitation characteristic and propulsion efficiency, it is important to analyze the characteristics of the normal force, thrust, speed, and slip to identify the optimal operating points. Nevertheless, the constant slip-frequency control has been applied as a control method in maglev trains because it can limit the vertical fore irrespective of the thrust and speed.

In this paper, the thrust and the normal force of the SLIM are analyzed at the available speed and slip ranges of rated voltage, using the 2-D finite-element method (FEM) analysis. A speed-slip condition with a stable normal force at the rated input is derived. Furthermore, the effectiveness of the slip limitation area is determined by analyzing the thrust and normal force according to the speed and slip. To verify the proposed slip pattern, the variation in the normal force is tested by implementing the general indirect field-oriented control (IFOC) and the constant slip-frequency indirect vector control (CSIFOC). The proposed algorithms are validated by simulation and by a full-sized SLIM experiment.

## II. Magnetic Field Analysis According to the Slip and Speed

### A. Analysis Model

A 200 km/h-class maglev train has six cars in one set, with each car having six bogies. The car length is 20 m, and the length of the SLIM is 2.5 m. A diagram of the semi-high-speed maglev train and the associated SLIM is shown in Fig. 1. The detailed specifications for the SLIM are listed in Table I. The motor is composed of 12 poles with 77 slots, and the required base velocity is 90 km/h.

### B. Rate-Characteristic Analysis

The base speed of the SLIM for the 200 km/h-class semi-high-speed maglev train is 90 km/h. The base speed is defined

Manuscript received March 16, 2018; revised May 6, 2018 and May 23, 2018; accepted May 24, 2018. Corresponding author: J.-H. Jeong (e-mail: tpts@cnu.ac.kr).

Color versions of one or more of the figures in this paper are available online at http://ieeexplore.ieee.org.

Digital Object Identifier 10.1109/TMAG.2018.2842222

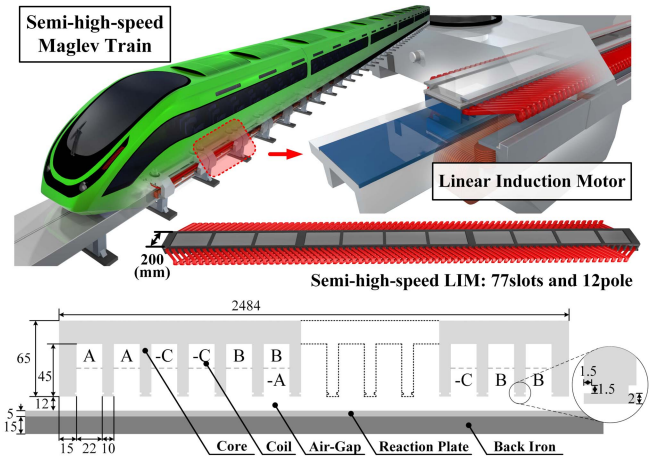


Fig. 1. Design specifications of LIM for the semi-high-speed maglev train.

TABLE I
DESIGN SPECIFICATIONS OF LIM FOR SEMI-HIGH-SPEED MAGLEV TRAIN

| Quantity | Value | Quantity | Value |
|---|---|---|---|
| Base speed | 90 (km/h) | Rate thrust | 3.25 (kN) |
| Output power | 81.25 (kW) | Line voltage | 424 (V) |
| Motor length | 2484 (mm) | Motor width | 200 (m) |
| Air gap | 12 (mm) | Conductor sheet | 5 (mm) |
| Turns per coil | 3 | Number of poles | 12 |

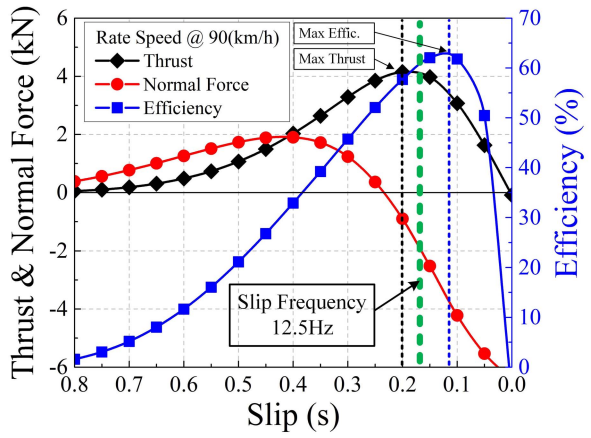


Fig. 2. Thrust, normal force, and efficiency with respect to the slip frequency.

as the maximum speed that can generate the required thrust in the SLIM speed-thrust characteristics. Thus, the motor characteristics are analyzed by FEM analysis up to the rated speed of 90 km/h. The thrust, normal force, and the efficiency analyzed with respect to the slip are shown in Fig. 2. According to the slip analysis, the maximum thrust is 4.1 kN at a slip of 0.2, and the maximum efficiency is approximately 63% at that of 0.12. The maximum thrust point and the maximum efficiency point have different slip values simultaneously. The slip point at the slip frequency of 12.5 Hz, in the graph, was determined as the acceptable operating point, at a speed of 90 km/h.

### C. Force Characteristics for the Slip and Speed Conditions

The normal force generated by the SLIM is a disturbance that affects the levitation system in a maglev train and can interfere with its stable operation. Therefore, the levitation stability of the train can be controlled by the accurate analyses

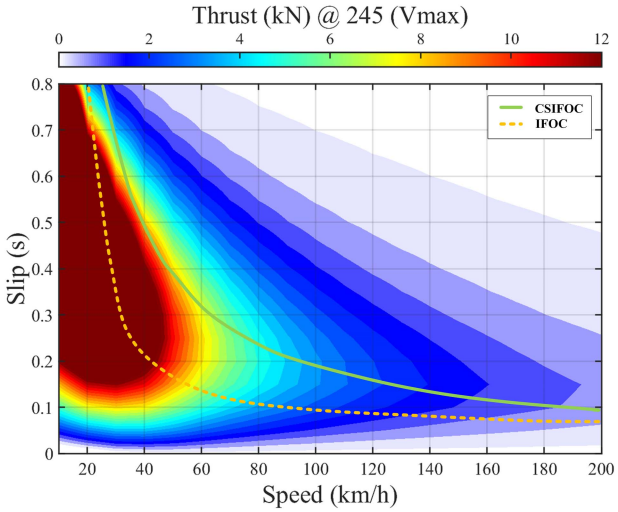


Fig. 3. Thrust analysis results according to the speed and slip.

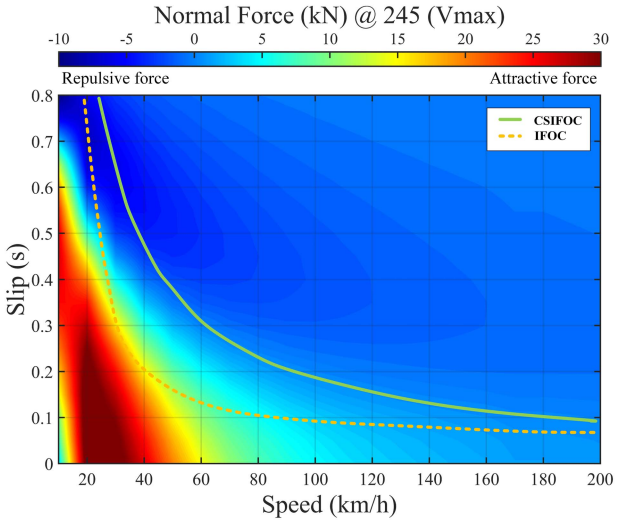


Fig. 4. Normal force analysis results according to the speed and slip.

of the normal force characteristics and applying it to the control strategy. Figs. 3 and 4 show the contour plots of the thrust and normal force characteristics, respectively. The analysis conditions are 245 Vmax for the input voltage and 160.5 Hz for the frequency. The thrust is shown with the slip lines of the CSIFOC and IFOC in Fig. 3. The slip lines of the two algorithms are shown through FEM analysis. The load thrust is 3 kN and the slip frequency of CSIFOC is 12.5 Hz. As shown, both algorithms satisfy the condition of 3.25-kN rated thrust, as shown in Table I. In Fig. 4, the slip lines of the two algorithms are compared with each other, and the CSIFOC generates a lower normal force than the IFOC. In conclusion, further CSIFOC operation can reduce the disturbance to the levitation system and improve the levitation reliability.

## III. SLIP-FREQUENCY CONTROL FOR A LOW NORMAL FORCE

### A. Equivalent Circuit of LIM

In this section, the previously interpreted FEM results are applied to the SLIM controller for analyzing the variation in the normal force. To implement the proposed algorithm

TABLE II
LIM EQUIVALENT CIRCUIT PARAMETERS

| Quantity | Value |
|---|---|
| $R_1$ | 0.012 (Ω) |
| $L_m$ | 0.93 (mH) |
| $R_2$ | 0.038 (Ω) |
| $L_2$ | 0.25 (mH) |

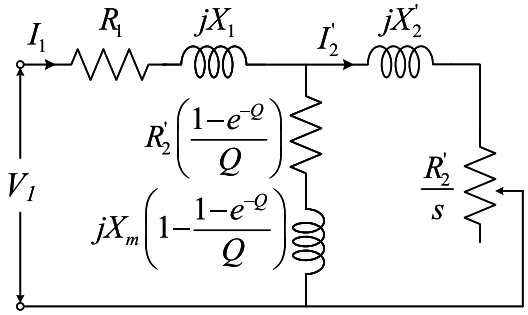


Fig. 5. Equivalent circuit of a semi-high speed maglev.

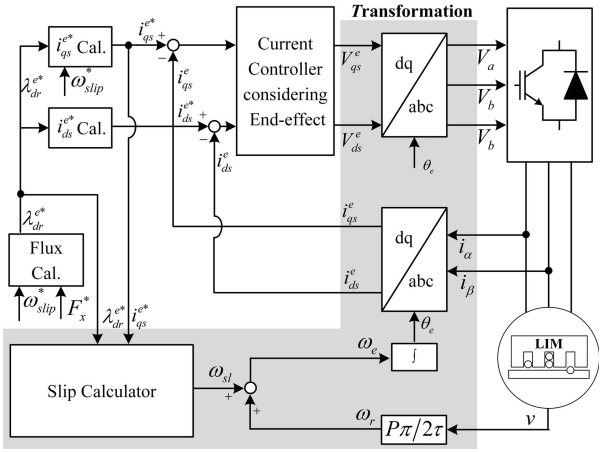


Fig. 6. Slip-controllable IFOC for a semi-high-speed maglev train.

for the SLIMs, the equivalent circuit parameters are required. Fig. 5 shows the equivalent circuit model for the SLIM by considering the end effects [5]. To derive the equivalent circuit parameters, the results of no-load, blocked-mover, and FEM analyses are applied. The derived circuit parameters are listed in Table II.

### *B. Indirect Vector Control for Constant Slip Frequency Control*

Fig. 6 is the block diagram of a slip-controllable IFOC-based control system. The steady-state force equation for the existing rotor, using field-oriented control, is as follows [6]:

$$F_x = \frac{3}{2}\frac{\pi}{\tau}\frac{P}{2}\frac{L_m(1-f(Q))}{L_{\rm lr}+L_m(f(Q))}\lambda^e_{\rm dr} i^e_{\rm qs} \tag{1}$$

where $F_x$ is the reference force for the speed, $\tau$ is the motor pole pitch, $P$ is the motor pole number, $L_m$ is the magnetizing inductance, $L_{\rm lr}$ is the secondary leakage inductance, $f(Q)$ is the end-effect function in [5], $\lambda^e_{\rm dr}$ is the secondary magnetic flux of the d-axis, and $i^e_{\rm qs}$ is the fixed-coordinate q-axis current reference

$$\omega^*_{\rm slip} = \frac{R_r(\hat{L}_m(1+f(Q))+\hat{L}_r)}{\hat{L}_r}\frac{i^e_{\rm qs}}{\lambda^e_{\rm dr}} \tag{2}$$

where $\omega^*_{\rm slip}$ is the slip angular velocity commend, and $R_r$ is the secondary resistance. $\hat{L}_r = L_{\rm lr} + \hat{L}_m$ is the secondary inductance. $\hat{L}_m = (1-f(Q))L_m$ is the magnetizing inductance considering the end effect. Substituting (2) into (1) and simplifying it yields the following commands for the CSIFOC current controller:

$$i^{e*}_{\rm qs} = \frac{\hat{L}_r}{R_r(L_m(1+f(Q)+\hat{L}_r)}\lambda^e_{\rm dr}\omega_{\rm slip} \tag{3}$$

$$i^{e*}_{ds} = \frac{R_r((1+f(Q)+p\hat{L}_r)}{L_m - L_r f(Q)}\lambda^{e*}_{\rm dr}. \tag{4}$$

## IV. EXPERIMENTAL ANALYSIS

### *A. Semi-High-Speed maglev Train Test Bed*

Fig. 7 shows the test bed used for verifying the proposed CSIFOC algorithm. The SLIM was equalized and fabricated as an arc type in a full- model size for a continuous test condition. Furthermore, an actual propulsion inverter of the maglev train was used for supplying the propulsion power. For the dynamo system, a rotary induction motor was used. A load cell was installed on top of the SLIM for measuring the normal force.

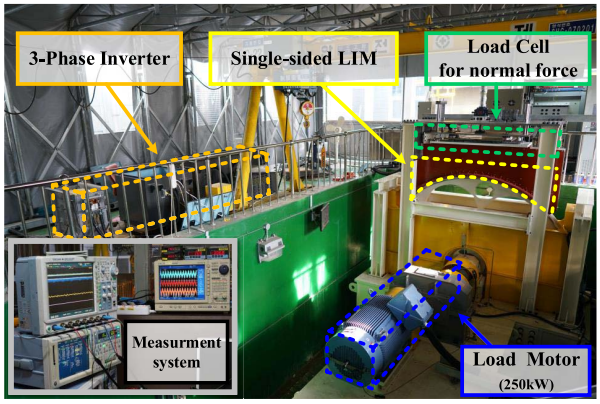


Fig. 7. Semi-high speed SLIM test bed.

### *B. Experimental Verification*

Experiments were performed with the same speed profile and thrust command to compare the proposed algorithm, the IFOC, and the CSIFOC. The experiments were performed within the 90 km/h region, which is the rated speed. A constant load thrust of 1 kN was applied. The driving pattern included acceleration, coasting, and deceleration, as shown in Fig. 8.

The experimental results are shown in Fig. 9. The IFOC's slip frequency was determined by the ratio of the D-axis and the Q-axis and has an asymmetrical shape. However, because the CSIFOC has a constant slip frequency, it has the same slip pattern in acceleration and deceleration. As in the FEM result of the normal force, the IFOC has a higher normal

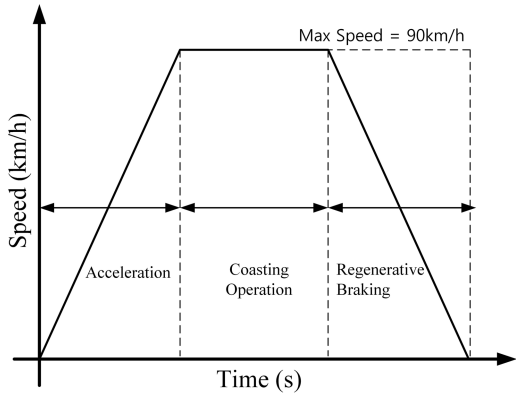


Fig. 8. Driving pattern for experiments.

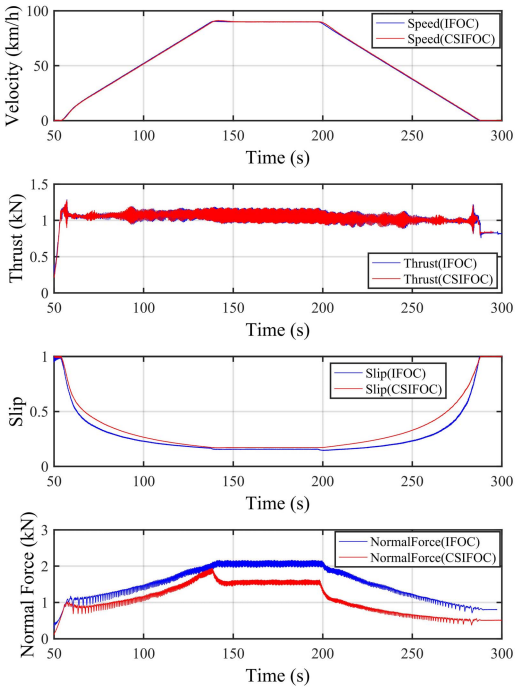


Fig. 9. Normal force dynamic experiment analysis.

force than the CSIFOC. It shows a more pronounced normal force reduction effect in the constant speed and deceleration operations.

Fig. 10 shows the result of the energy consumption according to the algorithms. The CSIFOC shows a lower energy consumption in the constant and deceleration speed regions, because the secondary plate of the LIM test apparatus is formed in a circular shape as in Fig. 7. In this structure, the higher normal force increases frictional losses in the rotational axis. Therefore, the CSIFOC, which has a relatively low load thrust and normal force, has a lower power consumption in the coasting and deceleration speed regions. In the low-speed region of the deceleration region, IFOC consumes lower energy than CSIFOC. Because the normal force difference still occurs, the amount of energy consumption is lower

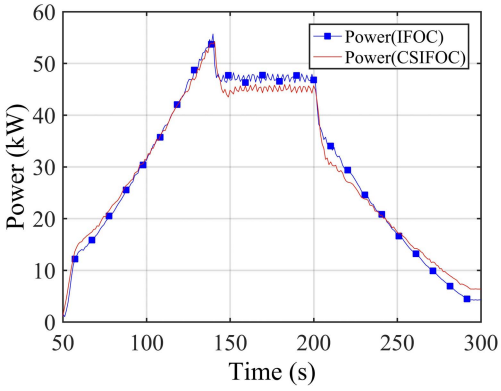


Fig. 10. Energy consumption of dynamic experiment.

due to slip different. However, in the acceleration region, the loss due to the normal force increase and the loss reduction due to the low slip are balanced, showing a similar power consumption pattern.

## V. Conclusion

We herein proposed a CSIFOC considering the normal force of an LIM. To obtain the slip frequency for the minimum normal force during operation, the thrust and the normal force of the LIM are obtained for the speed and slip using the 2-D FEM analysis. Based on the proposed slip, CSIFOC is proposed to change the slip according to the speed. The proposed algorithm reduces the force by up to 18% at a low-speed compablack with other algorithms through the actual 250 kW LIM. These results will help improve the safety and reliability of maglev trains. Furthermore, it is necessary to study the normal force in all areas of train operation through the normal force study in the weak field and regeneration areas.

## Acknowledgment

This work was supported by the National Research Council for Science and Technology within the project Development of Decentralized Levitation Control Technologies for Improved Reliability and Economic Feasibility.

## References

[1] I. Boldea, *Linear Electric Motors*, Englewood Cliffs, NJ, USA: Prentice-Hall, 2001.
[2] L. Yan, "Development and application of the Maglev transportation system," *IEEE Trans. Appl. Supercond.*, vol. 18, no. 2, pp. 92–99, Jun. 2008.
[3] B.-T. Ooi and D. C. White, "Traction and normal forces in the linear induction motor," *IEEE Trans. Power App. Syst.*, vol. PAS-89, no. 4, pp. 638–645, Apr. 1970.
[4] K. Wang, Y. Li, Q. Ge, and L. Shi, "Indirect field oriented control of linear induction motor based on optimized slip frequency for traction application," in *Proc. 18th Eur. Conf. Power Electron. Appl. (EPE ECCE Eur.)*, Sep. 2016, pp. 1–10.
[5] J. Duncan, "Linear induction motor-equivalent-circuit model," *IEE Proc.-Electr. Power Appl.*, vol. 130, no. 1, pp. 51–57, Jan. 1983.
[6] G. Kang and K. Nam, "Field-oriented control scheme for linear induction motor with the end effect," *IEE Proc.-Electr. Power Appl.*, vol. 152, no. 6, pp. 1565–1572, Nov. 2005.